Journal of the Geological Society, London, Vol. **170**, 2013, pp. 465–476. doi: 10.1144/jgs2012-037
Published *Online First* on April 22, 2013

Large sulphur isotopic perturbations and oceanic changes during the Frasnian–Famennian transition of the Late Devonian

DAIZHAO CHEN[1,*], JIANGUO WANG[1], GRZEGORZ RACKI[2], HUA LI[3], CHENGYUAN WANG[4], XUEPING MA[3] & MICHAEL T. WHALEN[5]

[1]*Key Laboratory of Petroleum Resources Research, Institute of Geology and Geophysics, Chinese Academy of Sciences, #19 Beitucheng Xilu, Chaoyang District, Beijing 100029, China*

[2]*Faculty of Earth Sciences, University of Silesia, Bedzinska Str. 60, 41-200 Sosnowiec, Poland*

[3]*Department of Geology, Peking University, Beijing 100871, China*

[4]*Nanjing Institute of Geology and Paleontology, Chinese Academy of Science, 39 East Beijing Road, Nanjing 210008, China*

[5]*Department of Geology and Geophysics, University of Alaska Fairbanks, Fairbanks, AK 99775, USA*

**Corresponding author (e-mail: dzh-chen@mail.iggcas.ac.cn)*

Abstract: The Frasnian–Famennian transition of the Late Devonian was one of the most critical intervals in the Phanerozoic. Sulphur isotopic pairs of carbonate-associated sulphate and pyrite sulphide from coeval sections in South China and Poland reveal frequent perturbations of sulphur cycling during this time interval. These data suggest a sudden oceanic overturn during a rapid sea-level fall probably induced by jerky block tilting in the latest Frasnian. This event was followed by long-lasting photic-zone euxinia during a rapid sea-level rise in the earliest Famennian. Large increases in continental nutrient fluxes, and subsequent primary productivity and organic burial, could have greatly enhanced bacterial sulphate reduction, producing excessive sulphide through the water columns owing to iron depletion. Subsequently, rapid ventilation of oceanic basins occurred, during which direct aerobic oxidation of sulphide into sulphate predominated in bottom waters and even surface sediments with minimal fractionation. This oxygenation was probably induced by intensive climatic cooling and/or large-scale sea-level fall. The temporal coincidence of two extinction phases with the oceanic overturn and succeeding photic-zone euxinia suggests that these extreme oceanic events played an important role in the severe biotic crisis. Furthermore, photic-zone euxinia coupled with subsequent climatic cooling may have delayed post-extinction recovery of some taxa.

Supplementary materials: Two supplementary tables (S1 and S2) indicating pyrite and CAS contents and sulphur isotopic results ($\delta^{34}S_{CAS}$, $\delta^{34}S_{py}$ and $\Delta^{34}S$) across the F-F boundary at Fuhe, South China and Kowala, Poland, respectively, and a supplementary figure showing systematic sulphur isotopic variations across the F-F boundary and their correlations between the two studied sections are available at www.geolsoc.org.uk/SUP18593.

The Late Devonian Frasnian–Famennian (F–F) biotic crisis, one of the five greatest Phanerozoic mass extinction events, is characterized by stepwise, most typically two-phase massive demises. During this crisis, *c*. 80% of marine faunal species, particularly shallow-water tropical species, were lost and did not recover until near the end of the Devonian (McGhee 1996; Bambach *et al*. 2004; Racki 2005). Various causes have been proposed for this critical event, of which oceanic anoxia is particularly favoured (Joachimski & Buggisch 1993; Algeo *et al*. 1995; Bond *et al*. 2004). Nevertheless, the mechanism, extent and timing of the anoxia remain uncertain (Racki 2005).

Oceanic anoxic events (OAEs) occur when the deep ocean becomes temporarily oxygen-depleted (e.g. Jenkyns 1980; Arthur & Sageman 1994). In some cases, hydrogen sulphide (H_2S) concentration builds up to a toxic level in the water column and anoxia evolves into euxinia (Meyer & Kump 2008). In anoxic zones of modern stratified lakes and restricted marine basins such as the Black Sea, conditions are favourable for bacterial sulphate reduction (BSR) to sulphide (Arthur & Sageman 1994; Kump *et al*. 2005). Because BSR favours the lighter and more weakly bonded isotope ^{32}S, the resulting sulphide is typically depleted in ^{34}S relative to coeval sulphate owing to substantial kinetic isotope fractionation (Kaplan & Rittenberg 1964; Canfield 2001). This fractionation is largely mediated by water sulphate concentration. The isotopic difference between coeval sulphate and sulphide is widely regarded as a proxy for the isotopic fractionation that accompanies BSR, and is useful for understanding the palaeoceanographic conditions, sedimentary sulphur cycling and the atmospheric O_2 levels in Earth history (Canfield 2001; Habicht & Canfield 2001; Habicht *et al*. 2002).

Numerous studies indicate that $\delta^{34}S$ values of carbonate-associated sulphate (CAS) can faithfully record the isotopic signatures of coeval seawater sulphate (Burdett *et al*. 1989; Hurtgen *et al*. 2002). This permits reconstruction of high-resolution, nearly continuous records of seawater sulphate evolution, the sedimentary sulphur cycle, and oceanic changes at particular time intervals (Newton *et al*. 2004; Bottrell & Newton 2006; Riccardi *et al*. 2006). Although a few low-resolution sulphur isotopic data for sulphides and sulphates have been reported across the F–F boundary (Geldsetzer *et al*. 1987; Wang *et al*. 1996; Joachimski *et al*. 2001; John *et al*. 2010), high-resolution sulphur isotopic data for both sulphate and sulphide have not previously been reported.

To improve understanding of oceanic sulphur cycling and palaeoceanographic changes during the Late Devonian F–F transition, we present high-resolution sulphur isotopic pairs of CAS and pyrite sulphide ($\delta^{34}S_{CAS}$ and $\delta^{34}S_{py}$) and relevant isotopic differences

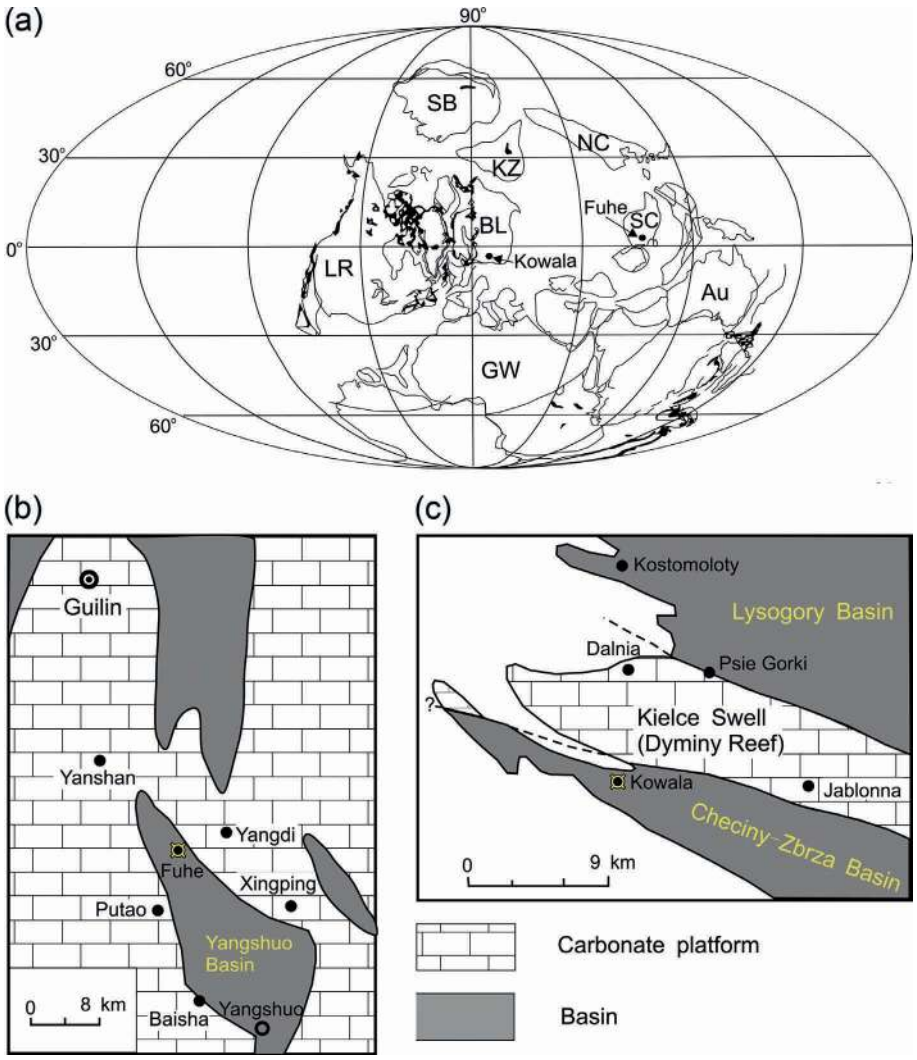

Fig. 1. (**a**) Palaeogeographical map for the Late Devonian. Shaded areas are mountain belts. SB, Siberia block; KZ, Kazakhstan block; BL, Baltic block; LR, Laurentian block; GW, Gondwana block; Au, Australia block; SC, South China block; NC, North China block (modified after Scotese & McKerrow 1990). (**b**) Tectono-depositional setting of studied section at Fuhe, Guilin, South China; (**c**) Tectono-depositional setting of studied section at Kowala, southern Poland. A platform is supposed to be located south of the Checiny–Zbrza basin and now is covered by Mesozoic strata (Racki 1993; Wojcik 2012).

$\Delta^{34}S$ (= $\delta^{34}S_{CAS} - \delta^{34}S_{py}$) in identical carbonate samples for this interval. Samples were collected at Fuhe (referred to as Yangdi in other literature), Guilin in South China, and at Kowala, Holy Cross Mountains in Poland. These correlative sites were located on the eastern and western sides of the Palaeo-Tethys Ocean (Fig. 1a) and therefore provide a cross-oceanic record of changes in ocean chemistry. Our data reveal perturbations in both $\delta^{34}S_{CAS}$ and $\delta^{34}S_{py}$ across the F–F boundary, in contrast to the low-resolution data of John *et al*. (2010), which were used as evidence against a change in sulphur cycling across this boundary. Based on these data, we present a new discussion on palaeoceanographic changes and cross-oceanic sulphur cycling and possible impacts on the severe biotic crisis during the F–F transition.

Geological background

The Fuhe section is located in a spindle- to rhomb-shaped transtensional (Yangshuo) interplatform basin surrounded by shallow carbonate platforms that restricted the water circulation and isolated the basin from continental influences (Fig. 1b; Chen *et al*. 2001, 2002). Within this basin, the F–F boundary succession is dominated by pelagic nodular limestones intercalated with calciturbidites and calcidebrites. Stratal cyclicity is well demonstrated in the deep-water deposits by decimetre-scale coarsening- or thickening-upward cycles that stack into metre-scale cycle-sets and larger-scale, third-order depositional sequences termed SFr and SFa (Fig. 2; Chen & Tucker 2003). Cycle stacking patterns indicate that cycles and cycle-sets were formed in response to the orbital perturbations of precession (16–18 kyr) and eccentricity (*c*. 100 kyr), respectively (Chen & Tucker 2003).

The Kowala section is located in a small semi-restricted to restricted intrashelf (half-graben?) basin (Checiny–Zbrza). This basin was bounded to the north by the Kielce Swell (Diminy Reef) and to the south by a platform that was subsequently buried under a Mesozoic succession (Fig. 1c; Racki 1993; Wojcik 2012). The F–F boundary succession is characterized by marly shales intercalated with thin- to medium-bedded limestones in which normally graded and hummocky cross-stratified beds are common (Fig. 3). Three lithological units, H2, H3 and H4, encompass the boundary succession (Fig. 3; Racki *et al*. 2002; Bond *et al*. 2004). Units H2 and H4 are characterized by outer-ramp rhythmic, dark greenish grey marlstone-dominated successions but unit H4 is more argillaceous. The middle H3 unit is characterized by reddish to pink, medium-bedded limestones with hummocky cross-stratification, indicating a shallower mid-ramp depositional setting. Coarsening- and cleaning-upward cycles are present and stack into larger-scale cycle-sets that are well correlated with those at Fuhe (Fig. 3).

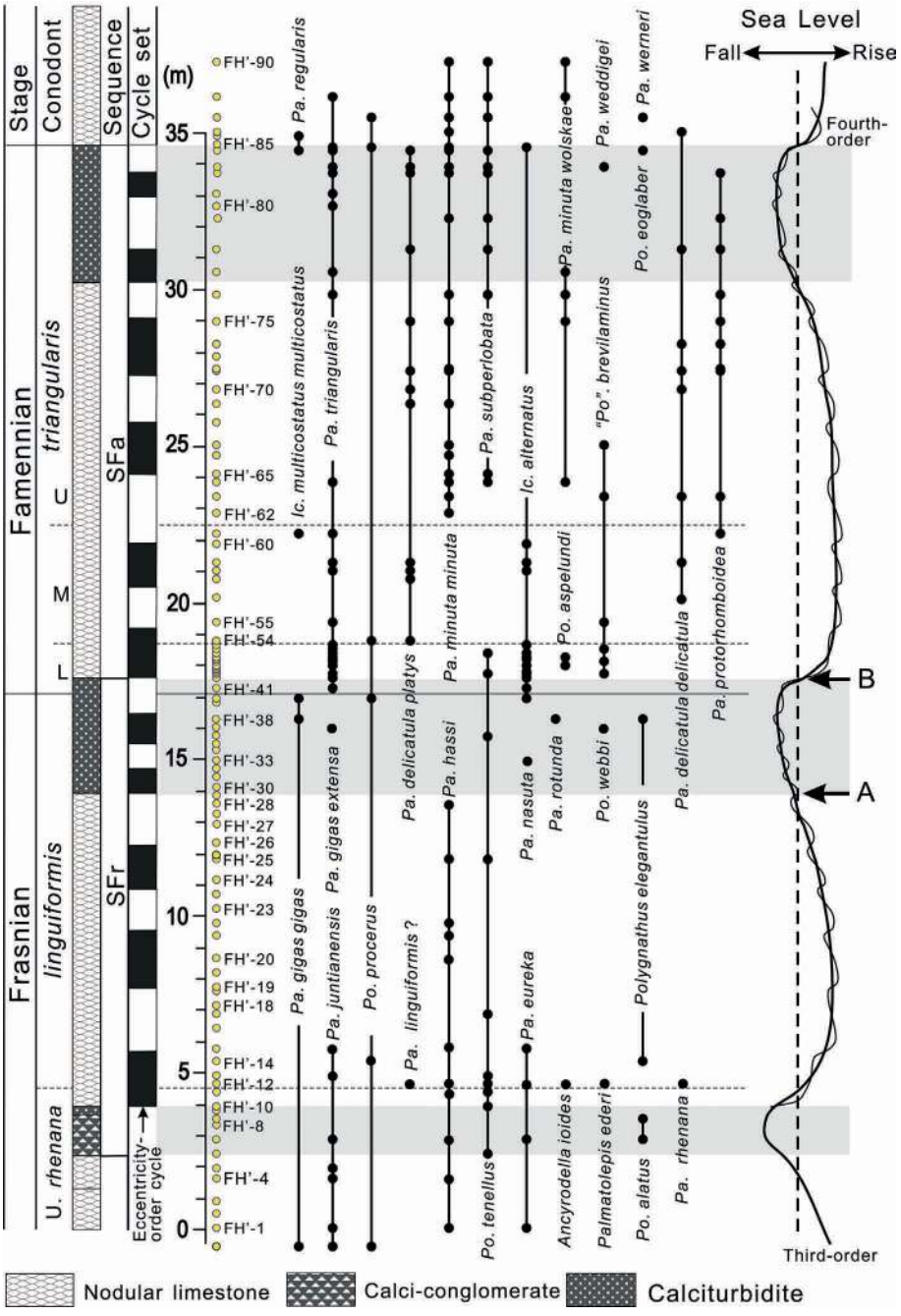

Fig. 2. Lithological succession and conodont zonation across the F–F boundary at Fuhe, South China. Vertical bars (black and white) on the right of the log mark the range of cycle-sets (eccentricity-driven cycles) (Chen & Tucker 2003). It should be noted that the F–F boundary is recalibrated by our new conodont data shown on the right. Relative sea-level changes of different orders are illustrated on the right. Arrows (A, B) mark the two phases of stepwise mass extinction during the F–F transition.

During the F–F transition, a third-order sea-level fall in the latest Frasnian (denoted interval I) is indicated by calcareous turbidite and tempestite packages at Fuhe and Kowala, respectively. This was followed by a sea-level rise (interval II) in the earliest Famennian. Higher-frequency sea-level fluctuations (fourth-order, *c*. 100 kyr) were superimposed on these longer-term events (Figs 2 and 3). Two phases (A and B) of massive biotic demise were temporally coincident with the onsets of third-order sea-level fall (interval I) and subsequent rise (interval II) at both localities (Racki *et al*. 2002; Chen & Tucker 2003).

Research methods

To better constrain the biostratigraphy of the F–F boundary at Fuhe, new conodont biostratigraphic work has been carried out and the conodont zonation was refined (Fig. 2). Within the high-resolution stratigraphic frameworks mentioned above, fresh micritic limestones distal to fractures were sampled for geochemical analysis. At Fuhe, the rock samples were derived from the sample sets of Chen *et al*. (2005).

Samples were first cut to remove the weathered surface and veins, and were examined microscopically. Chips without visible diagenetic euhedral pyrite crystals or their pseudomorphs were selected and then powdered. CAS was extracted for $\delta^{34}S_{CAS}$ analysis using modified methods from Burdett *et al*. (1989) and Hurtgen *et al*. (2002, 2006). Sample splits of 50−120 g were soaked in a 4−6% sodium hypochlorite solution for about 12 h to remove any metastable or organic sulphur compounds. The powder was rinsed multiple times with deionized water and then dissolved in a 25% HCl solution for 2–3 h. The insoluble residue

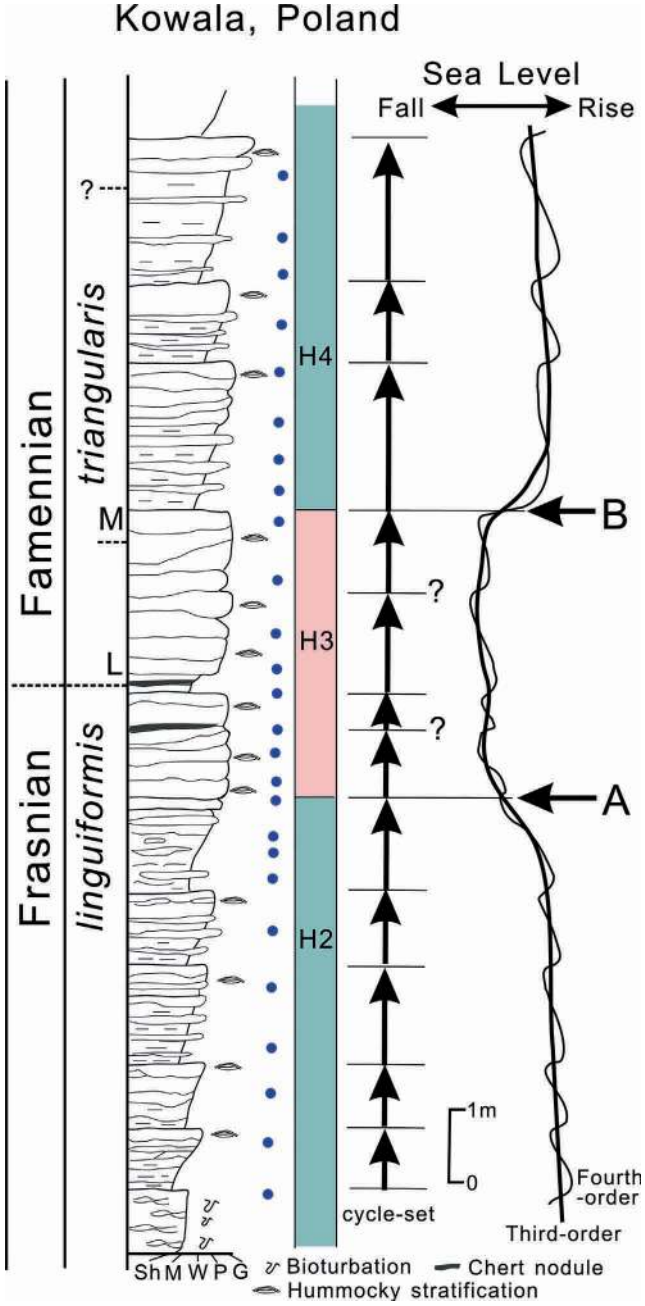

Fig. 3. Lithological succession (H2–H4) and depositional cyclicity across the F–F boundary at Kowala, Poland. Vertical arrows mark the extents of cycle-sets. Horizontal arrows (A, B) mark the major phases of stepwise biotic crisis during the transition. Relative sea-level changes of different orders are illustrated on the right. Filled dots are sampling positions. Sh, shale (or marly shale); M, mudstone; W, wackestone; P, packstone; G, grainstone.

was removed using 0.45 μm filters. Saturated $BaCl_2$ solution (10 ml, 10%) was added to the dissolved fraction to precipitate barite, which was heated for about 1 h and set aside for about 12 h. The barite was collected using the ashless filter paper. Barite (10–25 mg) was fully mixed with Cu_2O + quartz sand at 1:8:8 relative proportions in a tin capsule and combusted to 1200 °C in the presence of copper turnings. Resultant SO_2 gases were isolated cryogenically in a vacuum line and sealed in an ultrapure quartz tube.

Pyrite was extracted for $\delta^{34}S_{py}$ analysis using the chromium reduction method of Canfield *et al*. (1986). Sample splits of 10–20 g were treated with 100 ml $CrCl_2$ and concentrated HCl in a vessel and heated to about 120 °C for 1 h. The released H_2S was immediately purged via the N_2 carrier gas and bubbled into a mixed solution of 2% $AgNO_3$ and 6N NH_4OH, in which Ag_2S was precipitated and then filtered and weighed to calculate the pyrite concentration. Afterwards the precipitate (Ag_2S) was mixed with Cu_2O in a tin capsule and combusted to 1050 °C to produce SO_2 gases, which were isolated cryogenically in a vacuum line and sealed in an ultrapure quartz tube.

The purified SO_2 gases extracted from sulphate and pyrite were used to analyse the sulphur isotopic ratio in a Finnigan Delta-S mass spectrometer at the Institute of Geology and Geophysics, Chinese Academy of Sciences. The measurements were monitored and calibrated with NBS-127 and internal laboratory standards. Sulphur isotopic ratios are expressed using standard δ-notation relative to Vienna Cañon Diablo Troilite (VCDT) standard. The analytical reproducibility is better than ±0.2‰, based on repeated analysis of the standards.

Results

At Fuhe, the new conodont data pin the F–F boundary to near the top of the calciturbidite horizon of sequence SFr (Fig. 2), rather than at its top surface as proposed previously (Ji 1989). Paired $\delta^{34}S_{CAS}$–$\delta^{34}S_{py}$ and related $\Delta^{34}S$ values across the F–F boundary are presented for Fuhe (Fig. 4) and Kowala (Fig. 5). At Fuhe, coupled positive excursions of $\delta^{34}S_{CAS}$ and $\Delta^{34}S$ values are revealed at the base of interval I, which then shift back gradually through this interval, particularly for $\Delta^{34}S$ (Fig. 4). More prominently, subsequent coupled negative shifts of $\delta^{34}S_{CAS}$ and $\delta^{34}S_{py}$ pairs with relative low $\Delta^{34}S$ values appear and persist through interval II Subsequently, rapid coupled positive excursions of $\delta^{34}S_{CAS}$ and $\delta^{34}S_{py}$ pairs occur just above interval II (from upper *triangularis* subzone). However, the $\delta^{34}S_{CAS}$ values increase with a smaller magnitude and even decrease further upwards, thereby leading to an apparent decrease in $\Delta^{34}S$ (8.4‰) and subsequent transient negative $\Delta^{34}S$ interval (−1.6‰ to −4.1‰; Fig. 4). At Kowala, similar patterns of $\delta^{34}S_{CAS}$, $\delta^{34}S_{py}$ and $\Delta^{34}S$ are displayed with only minor differences; for example, the presence of a secondary coupled positive excursion of $\delta^{34}S_{CAS}$ and $\delta^{34}S_{py}$ values within interval II (Fig. 5). Therefore, at the two localities, the $\delta^{34}S_{CAS}$, $\delta^{34}S_{py}$ and $\Delta^{34}S$ values all show similar and significant fluctuations despite the wide separation of these localities across the Palaeo-Tethys Ocean (Fig. S1). However, the $\delta^{34}S_{py}$ and $\Delta^{34}S$ values generally display higher-frequency fluctuations than $\delta^{34}S_{CAS}$ values (Figs 4 and 5).

Evaluation of results

Pyrite oxidation during sample preparation

It is possible that the extracted CAS could be contaminated from pyrite oxidation during laboratory preparation (Marenco *et al*. 2008) or outcrop weathering. Weathering of pyrite would produce sulphate on rock surfaces or in fractures, but only freshly cut samples without fractures were prepared for powdering. Only carbonate samples with high pyrite content (i.e. >1.0 wt%) that were digested for longer than 8 h would have a potential risk of CAS contamination (Marenco *et al*. 2008; Kohl & Bao 2011). To reduce the risk of contamination resulting from pyrite

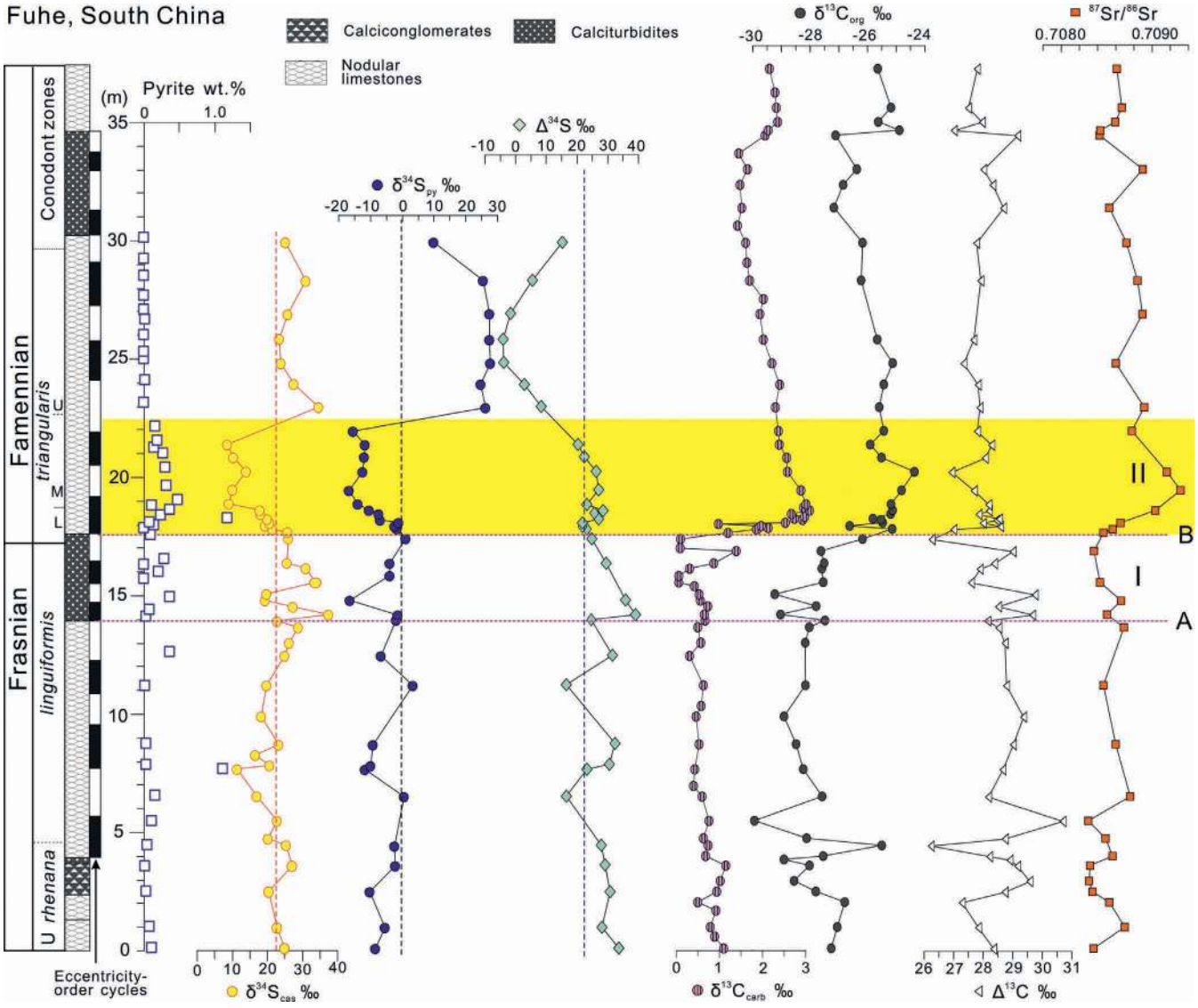

Fig. 4. Pyrite content and multiple isotopic (S–C–Sr) variations across the F–F boundary at Fuhe, South China. C–Sr isotopic data are from Chen *et al*. (2005). Vertical dashed lines mark the averages of sulphur isotopic values. Horizontal dashed lines mark the two main phases (A, B) of biotic crisis during the F–F transition.

oxidation during sample preparation, the HCl digestion was limited to 2–3 h.

At Fuhe, the pyrite concentration in our samples is mostly <0.5 wt% (Fig. 6a). Only two samples have pyrite contents close to 1.0 wt%, of which FH′-47 at the base of interval II yields the same $\delta^{34}S_{CAS}$ value as the surrounding low-pyrite samples (Fig. 4), implying minimal influence from pyrite oxidation. More generally, the inverse relationship between $\delta^{34}S_{CAS}$ and $\delta^{34}S_{py}$ values in the upper part of interval I mitigates against CAS contamination (Fig. 4), which would tend to produce a positive covariance. Although the weak covariances between pyrite concentration and $\delta^{34}S_{CAS}$ values ($R^2 = 0.23$; Fig. 6a) and between $\delta^{34}S_{py}$ and $\delta^{34}S_{CAS}$ values ($R^2 = 0.36$; Fig. 6b) could reflect an influence of pyrite oxidation during digestion, we will argue below that they actually represent primary signatures of palaeoceanographic conditions. If contamination did exist, CAS concentrations would increase in concert with pyrite contents, thereby causing a drawdown of the $\delta^{34}S_{CAS}$ value (Riccardi *et al*. 2006). However, the poor correlations between pyrite and CAS concentrations ($R^2 \approx 0$; Fig. 6c) and between CAS concentrations and $\delta^{34}S_{CAS}$ values ($R^2 \approx 0$; Fig. 6d) indicate negligible additions of sulphate from oxidized pyrite.

Although the pyrite concentrations at Kowala are more variable than those at Fuhe, they generally show the same trend; that is, they are extremely low in interval I and relatively high in intervals pre-I and II (Fig. 5). As at Fuhe, we interpret the weak to moderate correlations between pyrite concentration and $\delta^{34}S_{CAS}$ value($R^2 = 0.48$; Fig. 7a) and between $\delta^{34}S_{py}$ and $\delta^{34}S_{CAS}$ values ($R^2 = 0.21$; Fig. 7b) to result from palaeoceanographic conditions. Although low correlations are found in the cross-plots of pyrite and $\delta^{34}S_{CAS}$ v. CAS concentrations ($R^2 =$ 0.24 and 0.25; Fig. 7c and d respectively), the sample with the highest pyrite abundance (KW-20; 1.79 wt%) does not have the highest CAS concentration. Furthermore, sample KW-26, with the second highest content of pyrite (1.11 wt%), has the lowest CAS concentration and relatively high $\delta^{34}S_{CAS}$ value (Figs 5

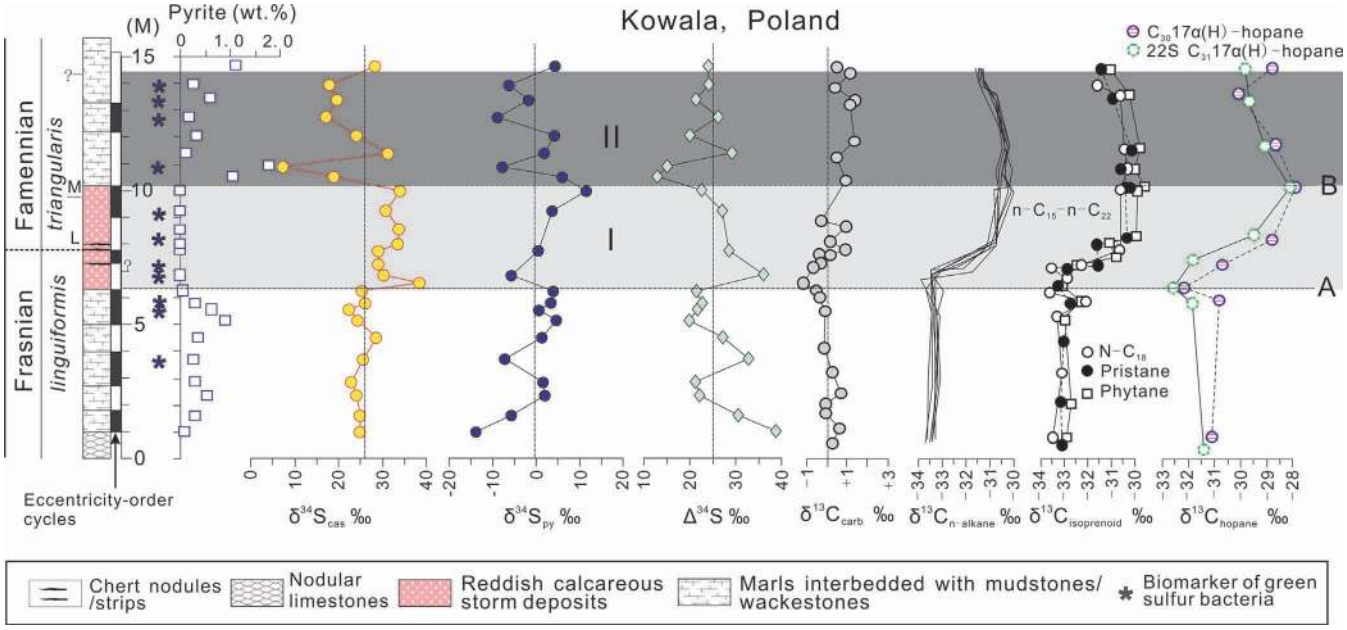

Fig. 5. Pyrite content and multiple isotopic (S–C) variations across the F–F boundary at Kowala, Poland. Carbon isotopic data are from Joachimski *et al*. (2001), who noted that the inorganic carbon data may have been influenced more or less by early diagenesis. Vertical dashed lines mark the averages of isotopic values. Two main phases of biotic crisis are marked by A and B.

and 7c, d). These negate any significant contamination of CAS by oxidized pyrite.

Diagenetic influences

It is necessary to consider the possibility that $\delta^{34}S_{CAS}$ values in the carbonates could have been altered during post-depositional diagenesis. The offshore basinal environments rule out penecontemporaneous meteoric recharge. Even if epigenetic meteoric processes did occur (i.e. along fracture networks), dissolution rather than precipitation of carbonates would prevail, such that textural alterations of impermeable host carbonates by meteoric fluids would be nearly impossible.

The samples for sulphur isotopic analysis are micrite-dominated, with very little organic matter, particularly those at Fuhe (Chen *et al*. 2005). Any petrographic textures associated with recrystallization, dolomitization and precipitation of secondary microspar to sparry calcite were excluded. Multiple isotopic ($\delta^{13}C_{carb}$, $\delta^{13}C_{org}$, $\delta^{18}O_{carb}$ and $^{87}Sr/^{86}Sr$ ratios) studies of carbonates were conducted at Fuhe by Chen *et al*. (2005), who found that primary seawater signals of $\delta^{13}C_{carb}$ and $\delta^{13}C_{org}$, and even the more diagenetically sensitive $^{87}Sr/^{86}Sr$ ratios, were preserved in carbonates. This study utilized the same sample sets, so it is reasonable to assume that diagenetic influences on $\delta^{34}S_{CAS}$ values were also negligible. The poor correlation between $\delta^{34}S_{CAS}$ and $\delta^{18}O_{carb}$ values in identical samples (Fig. 6e) further negates influence of meteoric or deep-burial diagenetic fluids that could have influenced $\delta^{34}S_{CAS}$ values.

Carbon isotope data from Kowala suggest that shallow-burial diagenesis may have occurred, especially in the organic-rich limestones (Joachimski *et al*. 2002). However, meteoric or deep-burial diagenetic rock–fluid interactions were almost negligible in view of the $\delta^{18}O_{carb}$ values of the limestones (−3.3‰ and −6.5‰, unpublished data), which are very close to those of coeval well-preserved brachiopod shells (Veizer *et al*. 1986). Therefore, the diagenetic influences on $\delta^{34}S_{CAS}$ values were minor; this is confirmed by the lack of evidence of allochthonous pore fluids displacing or mixing with residual seawaters in the formations.

Controls on sulphur cycling during the F–F transition

Oceanic chemistry and circulation

The weak to moderate covariance of pyrite contents and $\delta^{34}S_{CAS}$ values and that between $\delta^{34}S_{CAS}$ and $\delta^{34}S_{py}$ values shown in Figures 6 and 7 may partly reflect a low seawater sulphate level in the Late Devonian. Microbial culture experiments have shown that the degree of sulphur isotope fractionation that accompanies BSR in waters will decrease proportionally with sulphate concentration when it drops as low as 2 mM (Habicht *et al*. 2002). This scenario is also consistent with relative low concentrations of CAS and pyrite and high-frequency fluctuations in $\delta^{34}S_{CAS}$ and $\delta^{34}S_{py}$ in the F–F boundary carbonates (Figs 4 and 5), which indicate a short residence time for sulphate in the oceanic basins owing to a small reservoir and/or rapid flux (Ries *et al*. 2009). This hypothesis is further confirmed by the independent evidence from fluid inclusions of Late Devonian evaporites (*c*. 7 mM relative to *c*. 28 mM in the modern ocean; Lowenstein *et al*. 2003).

Furthermore, the semi-restricted to restricted basin morphology could have limited the lateral water circulation with the open sea (Fig. 1b, c) and further enhanced the oceanic stratification under the warm climate. This could have further aggravated intrabasinal sulphate depletion in view of the Devonian sulphate-depleted ocean. In such basins, progressive BSR would consume much of the available sulphate and lead to ^{34}S enrichment in that which remained. With insufficient replenishment, this would drive sulphur isotope compositions of both sulphate and sulphide proportionally to be heavier (Sælen *et al*. 1993; Habicht *et al*. 2002; Ries *et al*. 2009; Adams *et al*. 2010). Meanwhile, such small sulphate

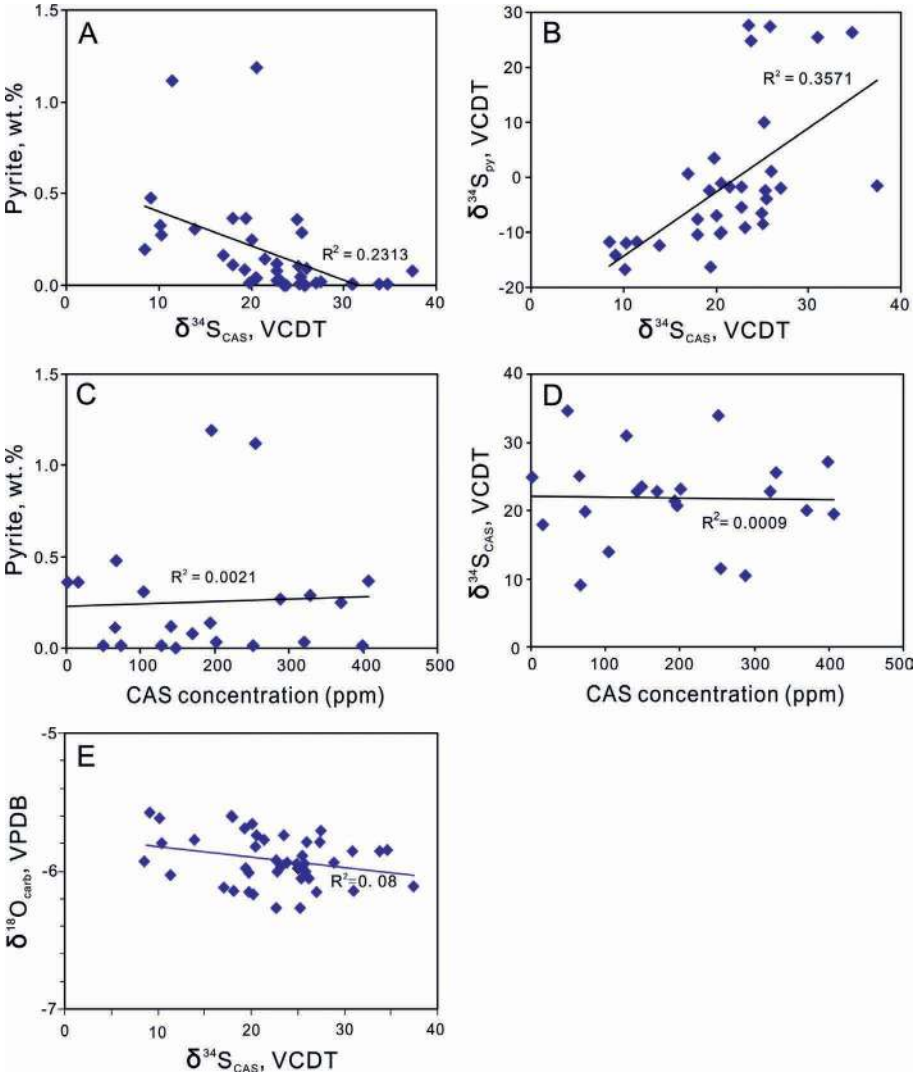

Fig. 6. (**a**) Cross-plot of $\delta^{34}S_{CAS}$ values and pyrite contents derived from insoluble residues after decarbonation at Fuhe (R^2 is correlation coefficient); (**b**) cross-plot of $\delta^{34}S_{CAS}$ and $\delta^{34}S_{py}$ values; (**c**) cross-plot of pyrite and CAS contents; (**d**) cross-plot of CAS concentrations and $\delta^{34}S_{CAS}$ values; (**e**) cross-plot of $\delta^{34}S_{CAS}$ and $\delta^{18}O_{carb}$ values of carbonates ($\delta^{18}O_{carb}$ data from Chen *et al*. 2005).

pools could be readily affected by allogenic factors (Adams *et al.* 2010), such as rapid sea-level fluctuations facilitating frequent perturbations in sulphur cycling, particularly in such restricted, small offshore basins without direct continental sulphur influx (Fig. 1a).

Oceanic overturn in the latest Frasnian

Coupled positive shifts in $\delta^{34}S_{CAS}$ and $\Delta^{34}S$ without apparent decrease in $\delta^{34}S_{py}$ occurred simultaneously at the two studied sections in the latest Frasnian at interval I (latest *linguiformis* zone; Figs 4 and 5). This scenario is inconsistent with the isotope mass balance that controls the sulphur isotope fractionation that accompanies BSR. During this process, the resulting sulphides are isotopically lighter than coeval sulphates, as observed in both laboratory experiments and modern oceans (Kaplan & Rittenberg 1964; Canfield 2001; Adams *et al.* 2010).

To better understand the context that resulted in the anomalous sulphur cycling at the onset of interval I, it is necessary to examine the sulphur cycling prior to this time. The decreases in $\Delta^{34}S$ values before this anomaly (Figs 4 and 5) indicate a synchronous drop in sulphate concentration in basins (e.g. Habicht *et al*. 2002). On the other hand, the coeval third-order sea-level highstand and slight fall (Figs 2 and 3) would have caused a lowering of the storm wave base and simultaneously enhanced carbonate production on platforms and shedding with ventilated waters into the restricted and anoxic basins. These may have forced contraction of anoxic waters downdip (Fig. 8a). In the decreased anoxic deep water bodies, the poorly renewed sulphate reservoir would become more exhausted and ^{34}S-enriched with depth owing to continuing BSR (Sælen *et al*. 1993; Adams *et al*. 2010). Pyrite formed in this evolved reservoir would become ^{34}S-enriched as well, and smaller $\Delta^{34}S$ values would result (Canfield 2001; Habicht *et al*. 2002).

At the base of interval I, the sharp larger-scale increase in $\delta^{34}S_{CAS}$ than $\delta^{34}S_{py}$ values and concomitant increase in $\Delta^{34}S$ values indicate a rapid rise in sulphate concentration in the studied basins. This paradoxical scenario may be explained by a catastrophic chemical overturn, which was proposed to account for the rapid positive $\delta^{34}S_{sulphate}$ excursion in oceanic basins particularly during the Late Devonian (Holser 1977; Goodfellow & Jonasson 1984; Strauss *et al*. 2001). However, the mechanism for triggering such an overturn has not been well documented. The occurrences of calciturbidites or calcidebrites and tempestites at the base of interval I reflect a sudden sea-level fall (Figs 2 and 3), which may have been further induced by block tilting in the context of extensional tectonism (Racki 1998; Chen *et al*. 2001, 2002; Chen & Tucker 2004). These factors could have

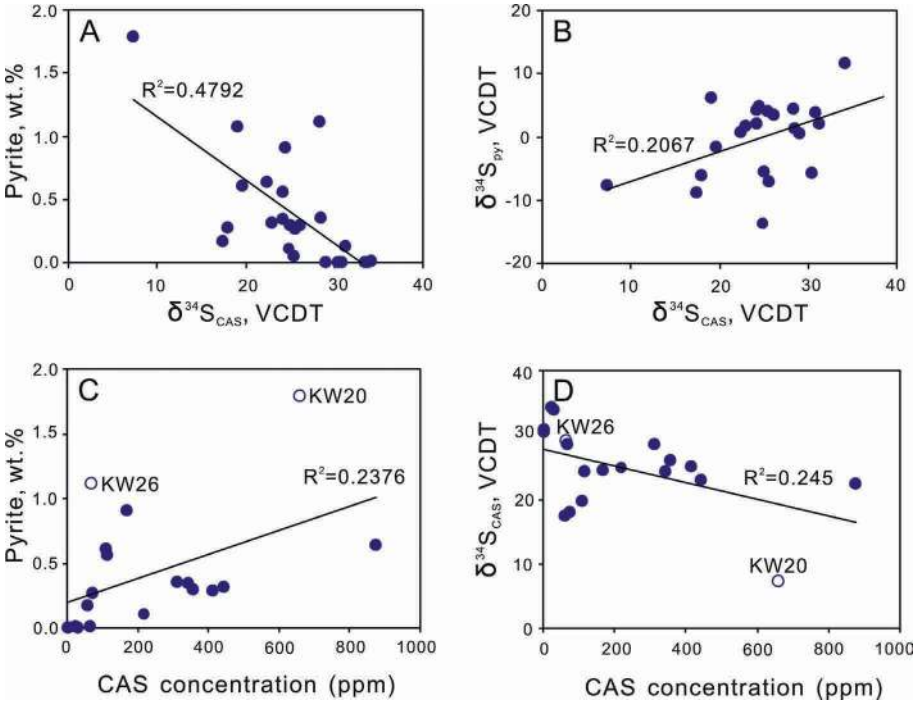

Fig. 7. (**a**) Cross-plot of $\delta^{34}S_{CAS}$ values and pyrite contents derived from insoluble residues after decarbonation at Kowala; (**b**) cross-plot of $\delta^{34}S_{CAS}$ and $\delta^{34}S_{py}$ values; (**c**) cross-plot of pyrite and CAS contents; (**d**) cross-plot of CAS concentrations and $\delta^{34}S_{CAS}$ values. The samples with relatively high pyrite contents (KW20 and KW26; open circles) are marked in (c) and (d).

enhanced mass flows on steep slopes and/or storm currents on mid- to outer ramps, and drove surface waters downward to the basin and bottom waters upwards to the surface, causing oceanic overturn (Fig. 8b). In this case, the oceanic stratification was temporarily upset and the sulphate within the basins was replenished so that the $\delta^{34}S_{CAS}$ values quickly returned to the values of a normal (or near-normal) oceanic system depending on the efficiency of watermass exchanges (Fig. 8b).

The coincidence of the $\delta^{34}S_{CAS}$ spike with the short-term negative $\delta^{13}C$ shift at the beginning of interval I at the two localities (Figs 4 and 5; Joachimski *et al*. 2001; Chen *et al*. 2005) is also in agreement with an oceanic overturn that drove the ^{12}C-enriched deeper waters upwards into the surface waters. At Kowala, the negative $\delta^{13}C$ shift of organic n-alkanes and isoprenoids derived from photoautotrophic eukaryotic algae, which prevailed in surface waters, is less apparent than that of hopanes derived from chemoautotrophic and heterotrophic eubacteria, which prevailed in deeper waters (Fig. 5). This pattern also supports an oceanic overturn. This short-term negative $\delta^{13}C$ perturbation is more apparent in the organic carbon dataset at the base of the prominent positive $\delta^{13}C$ excursion across the F–F successions at numerous localities (Joachimski & Buggisch 1993; Joachimski 1997; Murphy *et al*. 2000; Joachimski *et al*. 2002).

Enhanced productivity and oceanic euxinia in the earliest Famennian

The most prominent feature of sulphur cycling during the F–F transition is the large coupled negative $\delta^{34}S_{CAS}$ and $\delta^{34}S_{py}$ excursion in the earliest Famennian (interval II; Figs 4 and 5). This anomalous cycling accompanied the third-order sea-level rise (Figs 2 and 3) superimposed on a second-order sea-level highstand (Johnson *et al*. 1985). Examining published carbon and strontium isotopic data from the two sections (Joachimski *et al*. 2001, 2002; Racki *et al*. 2002; Chen *et al*. 2005), the coupled negative $\delta^{34}S$ excursions are coincident with the positive excursions of coupled $\delta^{13}C$ and $^{87}Sr/^{86}Sr$ ratios (Figs 4 and 5). This inverse relationship between sulphur and carbon cycling suggests that the ^{34}S-depleted sulphate pool was temporally associated with increased primary productivity and subsequent burial of organic carbon. The concomitant positive shift of $^{87}Sr/^{86}Sr$ ratios (Ebneth *et al*. 1997; Veizer *et al*. 1997; Chen *et al*. 2005) indicates that the enhanced bioproductivity was in turn induced by increased continental flux into marine basins. Furthermore, a third-order sea-level rise during this interval (Figs 2 and 3) indicates warm and humid climatic conditions. This scenario could have greatly enhanced hydrological cycling, chemical weathering and subsequent continental weathering flux (Weissert & Erba 2004). These processes are also in agreement with the context of broader geological processes including the landward colonization of vascular plants (Algeo *et al*. 1995). In these circumstances, the increased continental flux would have amplified the flux of isotopically light sulphur (average $\delta^{34}S_{weathering}$ *c*. 6‰; Adams *et al*. 2010) into marine basins, increasing the oceanic ^{34}S-depleted sulphate reservoir. This could have partially resulted in the coupled negative excursion of $\delta^{34}S_{CAS}$ and $\delta^{34}S_{py}$ pairs.

Increased primary productivity and burial of organic carbon in anoxic marine basins could have greatly enhanced BSR activity, producing voluminous amounts of H_2S. Some could be sequestered as pyrite in sediments and the remainder would have been released into the water column or even into the atmosphere depending on the Fe^{2+} availability. However, an apparent decrease in Fe availability and a slight increase in pyrite abundance in sediments are shown in interval II (Figs 4 and 5; Ma & Bai 2002; Racki *et al*. 2002; Pujol *et al*. 2006; Xu *et al*. 2008). This suggests an apparent enhanced BSR with an Fe deficiency so that most of the H_2S produced had not been sequestered in the form of pyrite. In such conditions, the excess H_2S gases were continuously released and diffused upwards into the photic zone, creating long-lasting photic-zone euxinia (i.e. Kump *et al*. 2005; Fig. 8c). This scenario is similar to the case of the late Cenomanian productivity-induced oceanic euxinia of the Cretaceous (Kuypers *et al*. 2002).

Photic-zone euxinia is also corroborated by the identification of biomarkers for the anoxygenic photosynthetic green sulphur bacteria

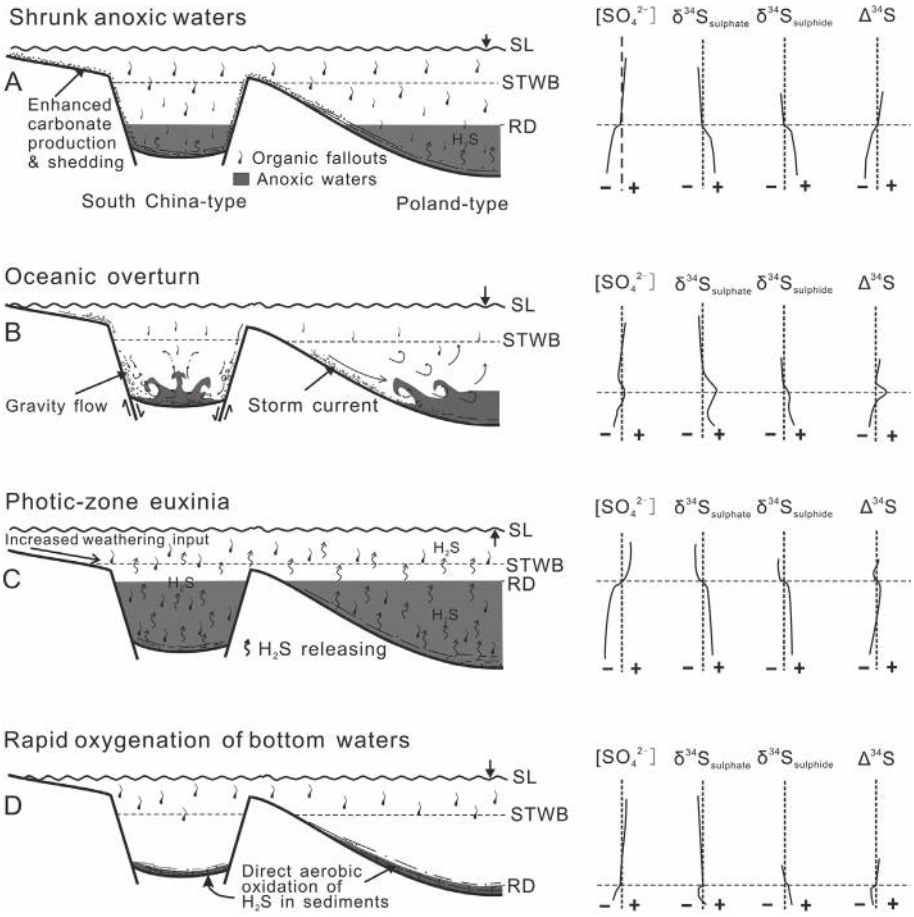

Fig. 8. Conceptual models of episodic oceanic changes (left) and sulphur cycling (right) during the F–F transition. The sulphur cycling around the redox interface should be noted. SL, sea level; STWB, storm wave base; RD, redox interface. **(a)** Shrunk areas of anoxic waters within basins during third-order sea-level highstand and slight fall. **(b)** Oceanic overturn during rapid sea-level drop possibly further induced by jerky block tilting. **(c)** Photic-zone euxinia during the third-order sea-level rise, and a warm and humid climate. The residence and direct oxidation of H_2S in the photic zone should be noted. **(d)** Rapid oxygenation of bottom waters during the strong climate cooling and sea-level fall.

in sediments of interval II. For example, at Kowala (Fig. 5), the presence of isorenieratane and its derivative has been recorded (Joachimski *et al*. 2001). Biomarkers of green sulphur bacteria in the equivalent horizons in North America (Brown & Kenig 2004) further confirm photic-zone euxinia there. Moreover, a delayed maximum of $\delta^{13}C_{org}$ versus $\delta^{13}C_{carb}$ data at Fuhe indicates a decreased carbon isotope difference between them (Fig. 4). This may be also contributed partly by green sulphur bacteria as a result of the low fractionation effect of carbon isotopes during anoxygenic metabolism (Van Breugel *et al*. 2005; Riccardi *et al*. 2007).

Furthermore, a high concentration of H_2S in the photic zone would favour direct oxidation of H_2S into sulphate by anoxygenic photosynthetic bacteria with very small fractionation (Fry *et al*. 1986; Habicht & Canfield 2001; Zerkle *et al*. 2009). This could have also contributed somewhat to the negative excursion of $\delta^{34}S_{CAS}$ and relatively low $\Delta^{34}S$ values imparted by the light isotopes of released H_2S (Figs 4 and 5). Therefore, the coupled negative excursion of $\delta^{34}S_{CAS}$ and $\delta^{34}S_{py}$ could have resulted from both increased weathering flux of isotopically light sulphur and reduced burial flux of pyrites (and/or increased H_2S release) owing to oceanic Fe^{2+} deficiency.

Although the massive burial of organic carbon could have induced subsequent climate cooling (Joachimski & Buggisch 2002), it may not have significantly influenced the chemical weathering and continental nutrient flux into oceans, especially in low-latitude areas. The delayed $^{87}Sr/^{86}Sr$ versus $\delta^{13}C_{carb}$ maxima is probably a reflection of this (Fig. 4; Chen *et al*. 2005). This condition could have sustained the high productivity and/or organic burial, and subsequent BSR-mediated H_2S production and build-up in water columns until near the nadir of climate cooling. During interval II, the coupled negative excursion of $\delta^{34}S_{CAS}$ and $\delta^{34}S_{py}$ values at Fuhe covers about three eccentricity-driven cycles (Fig. 4; Chen & Tucker 2003), implying persistence of the photic-zone euxinia, at least for *c*. 300 kyr. At Kowala, however, a short-term positive perturbation of $\delta^{34}S_{CAS}$ and $\delta^{34}S_{py}$ pairs is located in the upper part of a fourth-order depositional cycle within interval II (Fig. 5). This fact indicates that the transient 'heavy sulphur event' was temporally coincident with the shorter-term fourth-order sea-level fall during which the smaller and shallower basin was more ventilated by enhanced storm currents. In this case, the redox interface would have fallen below the sediment surface, leading to the isotopically heavy sulphur in the relatively closed pore waters in sediments owing to Rayleigh distillation.

Rapid oxygenation of oceanic basins in the early Famennian

Coupled positive excursions of $\delta^{34}S_{CAS}$ and $\delta^{34}S_{py}$ pairs are present at both localities above interval II, although only the initial portion is present at Kowala (Figs 4 and 5). In this 'sulphur heavy event', the magnitude of the $\delta^{34}S_{CAS}$ shift is lower than that of $\delta^{34}S_{py}$ (*c*. 25‰ v. *c*. 35‰), thus resulting in an apparent decrease in $\Delta^{34}S$ at the spike (8.4‰) and subsequent negative $\Delta^{34}S$ values (−1.6‰ to −4.1‰). This is in contrast to a sudden $\Delta^{34}S$ increase at the base of interval I (Fig. 4). $\Delta^{34}S$ values that accompany BSR are strongly influenced by sulphate availability; therefore a rapid decrease in

$\Delta^{34}S$ value indicates a large-scale drop in sulphate level (Canfield 2001; Habicht *et al*. 2002; Ries *et al*. 2009). This was unlikely to have been induced by oceanic overturn, which is proposed to cause the $\Delta^{34}S$ increase at the onset of interval I. The slight sea-level fall after interval II (Figs 2 and 4) could have lowered the storm wave base level and redox interface, resulting in a contraction of anoxic watermasses within the basins (Fig. 8a). This could readily result in a drawdown of the sulphate level through progressive BSR consumption and this may be the origin of coupled positive excursions of $\delta^{34}S_{CAS}$ and $\delta^{34}S_{py}$ pairs with decreased $\Delta^{34}S$ in the deep-water successions (Fig. 4; Habicht *et al*. 2002; Ries *et al*. 2009; Adams *et al.* 2010). However, the presence of negative $\Delta^{34}S$ values is puzzling, as sulphur isotope fractionation during BSR is generally greater than zero (2–45‰) even as the seawater sulphate concentration declines substantially (Kaplan & Rittenberg 1964; Habicht & Canfield 1997; Canfield 2001).

Such a paradox with negative $\Delta^{34}S$ values was also reported in the Neoproterozoic carbonates in NW China (Shen *et al*. 2008) and elsewhere (Ries *et al*. 2009). The former study proposed that sulphate and pyrite were derived from isotopically distinctive reservoirs in a chemically stratified basin or a basin with a sulphate minimum zone. In contrast, the latter study suggested that this scenario was caused by intense aerobic reoxidation of dissolved sulphide within sediments in very low sulphate waters, by which large negative $\Delta^{34}S$ values (average −8.2‰) were produced. The second scenario is probably more applicable to the current results. Laboratory work has shown that the sulphate produced by aerobic, abiotic oxidation of H_2S is depleted in ^{34}S (relative to the parent H_2S) by 4−5‰ (Fry *et al*. 1986, 1988). This could result in enriched $\delta^{34}S_{sulphide}$ relative to $\delta^{34}S_{sulphate}$ in the low-sulphate seawaters via Rayleigh-type distillation (Ries *et al*. 2009). The occurrence of pink to reddish nodular limestones in this negative $\Delta^{34}S$ interval (e.g. Chen *et al*. 2001; Chen & Tucker 2003) confirms coeval completely oxygenated bottom waters on the basin floor. The redox interface must therefore have moved further downwards beneath the sediment surface, so that almost all of the dissolved H_2S produced in the diminished sulphate-depleted anoxic pore waters could have been reoxidized before precipitation as pyrite, resulting in sulphate depleted in ^{34}S (or negative $\Delta^{34}S$ values; Figs 4 and 8d).

Recent geological evidence shows an onset of extensive glaciation on Gondwana probably from the late *triangularis* subzone of the early Famennian (Isaacson *et al*. 2008), which was probably temporally linked to this rapid oxygenation event. In this case, the glaciation-induced cooling could have driven more intense oceanic circulation by sinking of polar cold, dense and oxygen-enriched waters (e.g. Broecker 1997). The synchronous large-scale eustatic sea-level fall could also result in large-scale propagation of siliciclastic depositional systems into marine basins (e.g. Johnson *et al*. 1985; Isaacson *et al*. 2008). Both processes could have led to the rapid oxygenation of bottom waters of nearshore and offshore basins.

Implications for the biotic crisis during F–F transition

The F–F biotic crisis was characterized by two episodes of stepwise extinction: the first massive decline (A) in concert with the major sea-level fall (interval I) and a further demise (B) coincident with the subsequent major sea-level rise (interval II) (Chen & Tucker 2003; Figs 2 and 3). Our sulphur isotopic data suggest that oceanic overturn occurred at the onset of major sea-level fall and the long-lasting (*c*. 300 kyr) photic-zone euxinia took place during the major sea-level rise. The temporal coincidence of the biotic crises with sudden oceanic changes (physically and chemically) suggests a causal link.

The overturning of deep anoxic waters into the surface waters could have created detrimental ecological niches in shallow-water regimes, particularly along platform marginal zones where shallow-water benthic, notably reef-building organisms colonized. This condition could have resulted in anoxic suffocation of the benthos, leading to the initial mass die-offs (McGhee 1996; Racki 2005). The succeeding episodic hydrothermal (or volcanic) activity during interval I (Racki 1998; Ma & Bai 2002; Racki *et al*. 2002; Chen *et al*. 2005; Pujol *et al*. 2006; Xu *et al*. 2008) could have further degraded the fragile ecological conditions.

Our data suggest that the subsequent long-lasting photic-zone euxinia prevailed in the marginal basins across the Palaeo-Tethys Ocean, and similar conditions have been reported elsewhere around the world (Joachimsk & Buggisch 1993; Over 2002; Bond *et al*. 2004). This scenario could have created more fragile and harsher ecological conditions for the organisms. The substantially decreased benthos that colonized shallow waters with excessive H_2S would have been affected by olfactory nerve paralysis and blood anoxia (e.g. Kump *et al*. 2005). Moreover, the massive decline ended just prior to the latest photic-zone euxinia (interval II; Figs 4 and 5). This temporal relationship suggests that this extreme oceanic condition and subsequent severe climatic cooling could have further delayed the subsequent recovery until near the end of Devonian, at least for some taxa.

Conclusions

This study shows frequent anomalies of sulphur cycling and oceanic changes during the Late Devonian F–F transition in South China and Poland, based on the paired sulphur isotope data of CAS and pyrite in carbonates. The main conclusions drawn are as follows.

(1) In the latest Frasnian, the rapid sea-level fall that was induced possibly by block tilting could have enhanced turbidity and/or storm currents and thereby induced oceanic overturn in partially restricted, stratified and anoxic basins. This process could have driven the deep anoxic, ^{34}S-enriched watermasses depleted in sulphate upwards into surface waters and replenished the depleted sulphate pool within the basins, leading to coupled excursions of $\delta^{34}S_{CAS}$ and $\Delta^{34}S$.

(2) In the earliest Famennian, the subsequent large-scale sea-level rise under a warmer and humid climate would have enhanced hydrological cycling and chemical weathering, and greatly increased fluxes of oxidized pyrite (^{34}S-depleted sulphate) and nutrients into oceans, resulting in a high primary productivity and burial of organic matter. In this context, the greatly enhanced BSR activity would have produced excessive ^{34}S-depleted H_2S gases that diffused upwards into the shallow waters owing to the Fe depletion, creating severe photic-zone euxinia. The direct oxidation of isotopically light H_2S into sulphate through anoxygenic metabolism in photic zones, together with increased continental isotopically light sulphate flux, could have produced the coupled negative excursions of $\delta^{34}S_{CAS}$ and $\delta^{34}S_{py}$ pairs with relative low $\Delta^{34}S$ values.

(3) At the late *triangularis* subzone, onset of extensive Gondwana glaciation and major sea-level fall could have improved seawater circulation and shrunk the sulphate-depleted, anoxic deep watermasses in the silled basins, possibly causing complete oxygenation. This resulted in the sudden coupled positive excursions of $\delta^{34}S_{CAS}$ and $\delta^{34}S_{py}$ pairs with reduced, even negative $\Delta^{34}S$ values owing to

direct aerobic oxidation of sulphide into sulphate depleted in ^{34}S relative to the sulphide within sediments.

(4) The extreme oceanic events during the F–F transition were causally linked to the coeval severe biotic crisis. The overturn of anoxic deep waters to the surface could have caused suffocation of shallow-water benthos, leading to their first massive decline. The subsequent photic-zone euxinia would have resulted in a further demise for the benthos that were persistently exposed to the toxic H_2S gases, and delayed recovery, together with the succeeding severe climate cooling.

This research is supported by the National Natural Science Foundation of China (NSFC) (grant numbers 40673013, 40839907 and 41290260), and is also a contribution to the CAS/SAFEA International Partnership Program for Creative Research Teams and IGCP 580 project. F. Lu from the Guangxi Geological Survey is highly appreciated for extraction of the conodonts. F. Zhang and L. Feng are thanked for their assistance in laboratory work. The authors gratefully acknowledge the constructive comments from two referees (A. Fallick and an anonymous referee), and further inspiring comments and editorial help from the editor J. Hendry.

References

Adams, D.D., Hurtgen, M.T. & Sageman, B.B. 2010. Volcanic triggering of a biogeochemical cascade during Oceanic Anoxic Event 2. *Nature Geoscience*, **3**, 201–204.

Algeo, T.J., Berner, R.A., Maynard, J.B. & Scheckler, S.E. 1995. Late Devonian oceanic anoxic events and biotic crises: 'Rooted' in the evolution of vascular land plants? *GSA Today*, **5**, 65–67.

Arthur, M.A. & Sageman, B. 1994. Marine black shales: depositional mechanisms and environments of ancient deposits. *Annual Review of Earth and Planetary Sciences*, **22**, 499–551.

Bambach, R.K., Knoll, A.H. & Wang, S.C. 2004. Origination, extinction, and mass depletions of marine diversity. *Paleobiology*, **30**, 522–542.

Bond, D., Wignall, P.B. & Racki, G. 2004. Extent and duration of marine anoxia during the Frasnian–Famennian (Late Devonian) mass extinction in Poland, Germany, Austria and France. *Geological Magazine*, **141**, 173–193.

Bottrell, S.H. & Newton, R.J. 2006. Reconstruction of changes in sulphur cycling from marine sulphate isotopes. *Earth-Science Review*, **75**, 59–83.

Broecker, W.S. 1997. Thermohaline circulation, the Achilles' heel of our climate system: will man-made CO_2 upset the current balance? *Science*, **278**, 1582–1588.

Brown, T.C. & Kenig, F. 2004. Water column structure during the deposition of Middle Devonian–Lower Mississipian black and green/gray shales of the Illinois and Michigan Basins: A biomarker approach. *Palaeogeography, Paleoclimatology, Palaeoecology*, **215**, 59–85.

Burdett, J.W., Arthur, M.A. & Richardson, M. 1989. A Neogene seawater sulfur isotope age curve from calcareous pelagic microfossils. *Earth and Planetary Science Letters*, **94**, 189–198.

Canfield, D.E. 2001. Biogeochemistry of sulfur isotopes. *In*: Valley, J.W. & Cole, D. (eds) *Stable Isotope Geochemistry*. Mineralogical Society of America and Geochemical Society, Reviews of Mineralogy and Geochemistry, **43**, 607–636.

Canfield, D., Raiswell, R., Westrich, J., Reaves, C. & Berner, R. 1986. The use of chromium reduction in the analysis of reduced inorganic sulfur in sediments and shales. *Chemical Geology*, **54**, 149–155.

Chen, D. & Tucker, M.E. 2003. The Frasnian–Famennian mass extinctions: Insights from high-resolution sequence stratigraphy and cyclostratigraphy in South China. *Palaeogeography, Palaeoclimatology, Palaeoecology*, **193**, 87–111.

Chen, D. & Tucker, M.E. 2004. Palaeokarst and its implication for the extinction event at the Frasnian–Famennian boundary (Guilin, South China). *Journal of the Geological Society, London*, **161**, 895–898.

Chen, D., Tucker, M.E., Zhu, J. & Jiang, M. 2001. Carbonate sedimentation in a starved pull-apart basin, Middle to Late Devonian, southern Guilin, South China. *Basin Research*, **13**, 141–167.

Chen, D., Tucker, M.E., Zhu, J. & Jiang, M. 2002. Carbonate platform evolution: From a bioconstructed platform margin to a sand-shoal system (Devonian, Guilin, South China). *Sedimentology*, **49**, 737–764.

Chen, D., Qing, H. & Li, R. 2005. The Late Devonian Frasnian–Famennian (F/F) biotic crisis: Insights from $\delta^{13}C_{carb}$, $\delta^{13}C_{org}$, $^{87}Sr/^{86}Sr$ isotopic systematics. *Earth and Planetary Science Letters*, **235**, 151–166.

Ebneth, S., Diener, A., Buhl, D. & Veizer, J. 1997. Strontium isotope systematics of conodonts: Middle Devonian, Eifel Mountains, Germany. *Palaeogeography, Palaeoclimatology, Palaeoecology*, **132**, 79–96.

Fry, B., Cox, J., Gest, H. & Hayes, J.M. 1986. Discrimation between ^{34}S and ^{32}S during bacterial metabolism of inorganic sulphur compounds. *Journal of Bacteriology*, **165**, 328–330.

Fry, B., Ruf, W., Gest, H. & Hayes, J.M. 1988. Sulfur isotope effects associated with oxidation of sulfide by O_2 in aqueous solution. *Chemical Geology (Isotope Geoscience Section)*, **73**, 205–210.

Geldsetzer, H.H.J., Goodfellow, W.D., McLaren, D.J. & Orchard, M.J. 1987. Sulfur-isotope anomaly associated with the Frasnian–Famennian extinction, Medicine Lake, Alberta, Canada. *Geology*, **15**, 393–396.

Goodfellow, W.D. & Jonasson, I.R. 1984. Ocean stagnation and ventilation defined by $\delta^{34}S$ secular trends in pyrite and barite, Selwyn Basin, Yukon. *Geology*, **12**, 583–586.

Habicht, K.S. & Canfield, D.E. 1997. Sulfur isotope fractionation during bacterial sulfate reduction in organic-rich sediments. *Geochimica et Cosmochimica Acta*, **61**, 5351–5361.

Habicht, K.S. & Canfield, D.E. 2001. Isotope fractionation by sulfate-reducing natural populations and the isotopic composition of sulfide in marine sediments. *Geology*, **29**, 555–558.

Habicht, K.S., Gade, M., Thamdrup, B., Berg, P. & Canfield, D.E. 2002. Calibration of sulfate levels in the Archean ocean. *Science*, **298**, 2372–2374.

Holser, W.T. 1977. Catastrophic chemical events in the history of the ocean. *Nature*, **267**, 403–408.

Hurtgen, M.T., Arthur, M.A., Suits, N.S. & Kaufman, A.J. 2002. The sulfur isotopic composition of Neoproterozoic seawater sulfate: implications for a snowball Earth? *Earth and Planetary Science Letters*, **203**, 413–430.

Hurtgen, M.T., Halverson, G.P., Arthur, M.A. & Hoffman, P.F. 2006. Sulfur cycling in the aftermath of a 635-Ma snowball glaciation: Evidence for a syn-glacial sulfidic deep ocean. *Earth and Planetary Science Letters*, **245**, 551–570.

Isaacson, P.E., Díaz-Martínez, E., Grader, G.W., Kalvoda, J., Babek, O. & Devuyst, F.X. 2008. Late-Devonian–earliest Mississippian glaciation in Gondwanaland and its biogeographic consequences. *Palaeogeography, Palaeoclimatology, Palaeoeclogy*, **268**, 126–142.

Jenkyns, H.C. 1980. Cretaceous anoxic events: From continents to oceans. *Journal of the Geological Society, London*, **134**, 171–188.

Ji, Q. 1989. On the Frasnian–Famennian mass extinction event in South China. *Courier Forschungsinstitut Senckenberg*, **117**, 275–301.

Joachimski, M.M. 1997. Comparison of organic and inorganic carbon isotope patterns across the Frasnian–Famennian boundary. *Palaeogeography, Palaeoclimatology, Palaeoecology*, **132**, 133–145.

Joachimski, M.M. & Buggisch, W. 1993. Anoxic events in the late Frasnian: Causes of the Frasnian–Famennian faunal crisis? *Geology*, **21**, 675–678.

Joachimski, M.M. & Buggisch, W. 2002. Conodont apatite $\delta^{18}O$ signatures indicate climatic cooling as a trigger of the Late Devonian mass extinction. *Geology*, **30**, 711–714.

Joachimski, M.M., Ostertag-Henning, C., *et al*. 2001. Water column anoxia, enhanced productivity and concomitant changes in $\delta^{13}C$ and $\delta^{34}S$ across the Frasnian–Famennian boundary (Kowala–Holy Cross Mountains/Poland). *Chemical Geology*, **175**, 109–131.

Joachimski, M.M., Pancost, R.D., Freeman, K.H., Ostertag-Henning, C. & Buggisch, W. 2002. Carbon isotope geochemistry of the Frasnian–Famennian transition. *Palaeogeography, Palaeoclimatology, Palaeoecology*, **181**, 91–109.

John, E.H., Wignall, P.B., Newton, R.J. & Botrell, S.H. 2010. $\delta^{34}S_{CAS}$ and $\delta^{18}O_{CAS}$ records during the Frasnian–Famennian (Late Devonian) transition and their bearing on mass extinction models. *Chemical Geology*, **275**, 221–234.

Johnson, J.G., Klapper, G. & Sandberg, C.A. 1985. Devonian eustatic fluctuations in Euramerica. *Geological Society of America Bulletin*, **96**, 567–587.

Kaplan, I.R. & Rittenberg, S.C. 1964. Microbiological fractionation of sulphur isotopes. *Journal of General Microbiology*, **34**, 195–212.

Kohl, I. & Bao, H.M. 2011. Triple-oxygen-isotope determination of molecular oxygen incorporation in sulfate produced during abiotic pyrite oxidation (pH = 2–11). *Geochimica et Cosmochimica Acta*, **75**, 1785–1798.

Kump, L.R., Pavlov, A. & Arthur, M.A. 2005. Massive release of hydrogen sulfide to the surface ocean and atmosphere during intervals of oceanic anoxia. *Geology*, **33**, 397–400.

Kuypers, M.M., Pancost, R., Nijenhuis, I.A. & Sinninghe Damste, J.S. 2002. Enhanced productivity led to increased organic carbon burial in the euxinic North Atlantic basin during the late Cenomanian oceanic anoxic event. *Paleoceanography*, **17**, 1051, doi:1029/2000PA000569.

Lowenstein, T.K., Hardie, L.A., Timofeeff, M.N. & Demicco, R.V. 2003. Secular variation in seawater chemistry and the origin of calcium chloride basinal brines. *Geology*, **31**, 857–860.

Ma, X.P. & Bai, S.L. 2002. Biological, depositional, microspherule and geochemical records of the Frasnian/Famennian boundary beds, South China. *Palaeogeography, Palaeoclimatology, Palaeoecology*, **181**, 325–346.

Marenco, P.J., Corsetti, F.A., Hammond, D.E., Kaufman, A.J. & Bottjer, D.J. 2008. Oxidation of pyrite during extraction of carbonate associated sulfate. *Chemical Geology*, **247**, 124–132.

McGhee, G.R., Jr. 1996. *The Late Devonian Mass Extinction: The Frasnian/Famennian Crisis*. Columbia University Press, New York.

Meyer, K.M. & Kump, L.R. 2008. Oceanic euxinia in Earth History: causes and consequences. *Annual Review of Earth and Planetary Sciences*, **36**, 251–288.

Murphy, A.E., Sageman, B.B. & Hollander, D.J. 2000. Eutrophication by decoupling of the marine biogeochemical cycles of C, N, and P: A mechanism for the Late Devonian mass extinction. *Geology*, **28**, 427–430.

Newton, R.J., Pevitt, E.L., Wignall, P.B. & Bottrell, S.H. 2004. Large shifts in the isotopic composition of seawater sulphate across the Permian–Triassic boundary in northern Italy. *Earth and Planetary Science Letters*, **218**, 331–345.

Over, J. 2002. The Frasnian/Famennian boundary in central and eastern United States. *Palaeogeography, Palaeoclimatology, Palaeoecology*, **181**, 153–169.

Pujol, F., Berner, Z. & Stüben, D. 2006. Palaeoenvironmental changes at the Frasnian/Famennian boundary in key European sections: Chemostratigraphic constraints. *Palaeogeography, Palaeocimatology, Palaeocology*, **240**, 120–145.

Racki, G. 1993. Evolution of the bank to reef complex in the Devonian of the Holy Cross Mountains. *Acta Palaeontologica Polonica*, **37**, 87–182.

Racki, G. 1998. Frasnian–Famennian biotic crisis: Undervalued tectonic control? *Palaeogeography, Palaeoclimatology, Palaeoecology*, **141**, 177–198.

Racki, G. 2005. Towards understanding Late Devonian global events: few answers, many questions. *In*: Over, D.J., Morrow, J.R. & Wignall, P.B. (eds) *Understanding Late Devonian and Permian–Triassic Biotic and Climatic Events: Towards an Integrated Approach*. Developments in Palaeontology and Stratigraphy Series, **20**, 5–36.

Racki, G., Racka, M., Matyja, H. & Devleeschouwer, X. 2002. The Frasnian/Famennian boundary interval in the South Polish–Moravian shelf basins: Integrated event–stratigraphical approach. *Palaeogeography, Palaeoclimatology, Palaeoecology*, **181**, 251–297.

Riccardi, A.L., Arthur, M.A. & Kump, L.R. 2006. Sulfur isotopic evidence for chemocline upward excursions during the end-Permian mass extinction. *Geochimica et Cosmochimica Acta*, **70**, 5740–5752.

Riccardi, A.L., Kump, L.R., Arthur, M.A. & D'hondt, S. 2007. Carbon isotopic evidence for chemocline upward excursions during the end-Permian event. *Palaeogeography, Palaeoclimatology, Palaeoecology*, **248**, 73–81.

Ries, J.B., Fike, D.A., Pratt, L.M., Lyons, T.W. & Grotzinger, J.P. 2009. Superheavy pyrite ($\delta^{34}S_{pyr} > \delta^{34}S_{CAS}$) in the terminal Proterozoic Nama Group, southern Nambia; A consequence of low seawater sulfate at the dawn of animal life. *Geology*, **37**, 743–746.

Sælen, G., Raiswell, R., Talbot, M.R., Skei, J.M. & Bottrell, S.H. 1993. Heavy sedimentary sulfur isotopes as indicators of super-anoxic bottom-water conditions. *Geology*, **21**, 1091–1094.

Scotese, C.R & McKerrow, W.S. 1990. Revised world maps and introduction. *In*: McKerrow, W.S. & Scotese, C.R. (eds) *Palaeozoic Palaeogeography and Biogeography*. Geological Society of America, Memoirs, **12**, 1–12.

Shen, B., Xiao, S.H., Kaufman, A., Bao, H.M., Zhou, C.M. & Wang, H.F. 2008. Stratification and mixing of a post-glacial Neoproteroic ocean: Evidence from carbon and sulfur isotopes in a cap dolostone from northwest China. *Earth and Planetary Science Letters*, **265**, 209–228.

Strauss, H., Banerjee, D.M. & Kumar, V. 2001. The sulfur isotopic composition of Neoproterozoic to early Cambrian seawater—evidence from the cyclic Hanseran evaporites, NW India. *Chemical Geology*, **175**, 17–28.

Van Breugel, Y., Schouten, S., Paetzel, M., Ossebaar, J. & Sinninghe Damsté, J.S. 2005. Reconstruction of $\delta^{13}C$ of chemocline CO_2 (aq) in past oceans and lakes using the $\delta^{13}C$ of fossil isorenieratene. *Earth and Planetary Science Letters*, **235**, 421–434.

Veizer, J., Fritz, P. & Jones, B. 1986. Geochemistry of brachiopods: Oxygen and carbon isotopic records of Paleozoic oceans. *Geochimica et Cosmochimica Acta*, **50**, 1679–1696.

Veizer, J., Buhl, D., *et al*. 1997. Strontium isotope stratigraphy: Potential resolution and event correlation. *Palaeogeography, Palaeoclimatology, Palaeoecology*, **132**, 65–77.

Wang, K., Geldsetzer, H.H.J., Goodfellow, W.D. & Krouse, H.R. 1996. Carbon and sulfur isotope anomalies across the Frasnian–Famennian extinction boundary, Alberta, Canada. *Geology*, **24**, 187–191.

Weissert, H. & Erba, E. 2004. Volcanism, CO_2 and palaeoclimate: Late Jurassic–Early Cretaceous carbon and oxygen isotope record. *Journal of the Geological Society, London*, **161**, 695–702.

Wojcik, K. 2012. Famennian Fusulinina (Foraminifera) from the Holy Cross Mountains (central Poland). *Geological Journal*, doi:10.1002/gj.2419.

Xu, B., Gu, Z.Y., Han, J.T. & Wang, C.Y. 2008. Environmental changes during Frasnian–Famennian transition in south China: A multiproxy approach. *Journal of Geophysical Research*, **113**, G04033, doi:10.1029/2007JG000450.

Zerkle, A.L., Farquhar, J., Johnston, D.T., Cox, R.P. & Canfield, D.E. 2009. Fractionation of multiple sulfur isotopes during phototrophic oxidation of sulfide and elemental sulfur by a green sulfur bacterium. *Geochimica et Cosmochimica Acta*, **73**, 291–306.

Received 23 December 2012; revised typescript accepted 20 March 2012.
Scientific editing by James Hendry.